JACS
JOURNAL OF THE AMERICAN CHEMICAL SOCIETY
Article
pubs.acs.org/JACS

# Mononuclear Single-Molecule Magnets: Tailoring the Magnetic Anisotropy of First-Row Transition-Metal Complexes

Silvia Gomez-Coca,[†] Eduard Cremades,[†] Núria Aliaga-Alcalde,[‡,§] and Eliseo Ruiz*,[†]

[†]Departament de Química Inorgànica and Institut de Recerca de Química Teòrica i Computacional and [‡]Institució Catalana de Recerca i Estudis Avançats (ICREA) and Departament de Química Inorgànica, Universitat de Barcelona, Diagonal 645, E-08028 Barcelona, Spain

[§]ICREA - Institut de Ciència de Materials de Barcelona (ICMAB-CSIC), Campus de la UAB, 08193 Bellaterra, Spain

Supporting Information

**ABSTRACT:** Magnetic anisotropy is the property that confers to the spin a preferred direction that could be not aligned with an external magnetic field. Molecules that exhibit a high degree of magnetic anisotropy can behave as individual nanomagnets in the absence of a magnetic field, due to their predisposition to maintain their inherent spin direction. Until now, it has proved very hard to predict magnetic anisotropy, and as a consequence, most synthetic work has been based on serendipitous processes in the search for large magnetic anisotropy systems. The present work shows how the property can be predicted based on the coordination numbers and electronic structures of paramagnetic centers. Using these indicators, two $Co^{II}$ complexes known from literature have been magnetically characterized and confirm the predicted single-molecule magnet behavior.

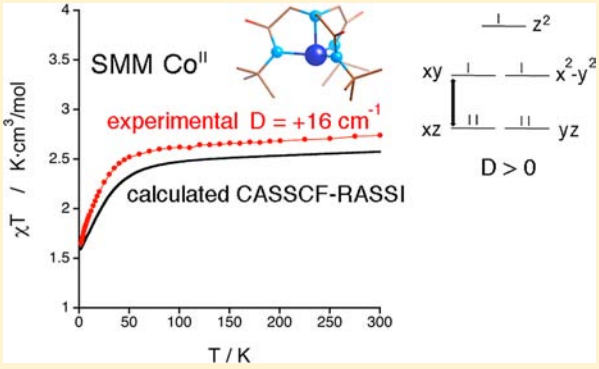


## INTRODUCTION

During recent decades considerable effort has been made to produce molecular materials that could behave as small nanomagnets (single-molecule magnets, SMMs).[1,2] In general, such systems are polynuclear transition-metal complexes that exhibit slow relaxation of their magnetization, which is essentially controlled by an energy barrier that may fix the spin direction. The following spin Hamiltonian gives the zero-field splitting (ZFS) terms that involve magnetic anisotropy:

$$\hat{H} = D\left(\hat{S}_z^2 - \frac{1}{3}\hat{S}^2\right) + E(\hat{S}_x^2 - \hat{S}_y^2) \quad (1)$$

where $D$ stands for the axial ZFS parameter (related to the anisotropy of the system) and $\hat{S}$ ($\hat{S}_i$) is the total spin operator (and the operators of its components) of the molecule.[3] The height of the magnetic anisotropy barrier depends on the total spin of the system and is given by the product $|D|\cdot S^2$ ($|D|\cdot S^2 - {}^1/_4$ for half-integer systems). The spin direction may be flipped (relaxation process) due to thermal crossing of the barrier or thermal-assisted tunnelling effects usually quantified by $E$, the rhombic ZFS parameter. SMM behavior has two specific characteristics that have been well-described in the past: steps in the hysteresis loops due to tunnelling effects and frequency dependence of the imaginary part of the magnetic susceptibility using ac magnetic fields. From a practical point of view, the frequency dependence of the imaginary part was employed to assign SMM behavior because in many cases it is technically difficult to characterize the hysteresis steps. The presence of tunnelling effects causes the real measured barrier ($U_{eff}$) to be smaller than the maximum value $|D|\cdot S^2$. Since Sessoli et al.[4] detected SMM behavior for the first time at a low temperature in a $[Mn_{12}O_{12}(CH_3COO)_{16}(H_2O)_4]$ complex usually known as $Mn_{12}(8Mn^{III}4Mn^{IV})$, many research groups have been searching for new polynuclear systems with large barriers in the hope of devising high-temperature applications (as current SMMs normally only function below 10 K). In general, the goal was to increase the total spin of the molecules ($S$) by adding more paramagnetic centers to the complexes together with seeking parallel alignment among the spins (ferromagnetic coupling), but this has not provided improved materials.[5] Best results for polynuclear systems containing first-row transition metals were obtained in 2007 with a $Mn_6$ complex, $[Mn_6O_2(Et\text{-}sao)_6(PhCOO)_2]$ (Et-sao: ethyl-salicylaldoxime), with six $Mn^{III}$ cations, achieved by Brechin and co-workers[6,7] which slightly overcomes the barrier of the original $Mn_{12}$ complex. Meanwhile the magnetic anisotropy quantified by the $D$ parameter (which depends on the spin−orbit contribution) is in principle a difficult property to predict and/or control. Hence, in many cases, as in those mentioned above, $Mn^{III}$ cations were routinely employed as the source of magnetic anisotropy.[8]

In 2003 a mononuclear complex $[TbPc_2]^-$ containing one $Tb^{III}$ cation was reported[9] to exhibit slow magnetization

Received: February 11, 2013
Published: April 16, 2013

   dx.doi.org/10.1021/ja4015138 | J. Am. Chem. Soc. 2013, 135, 7010−7018

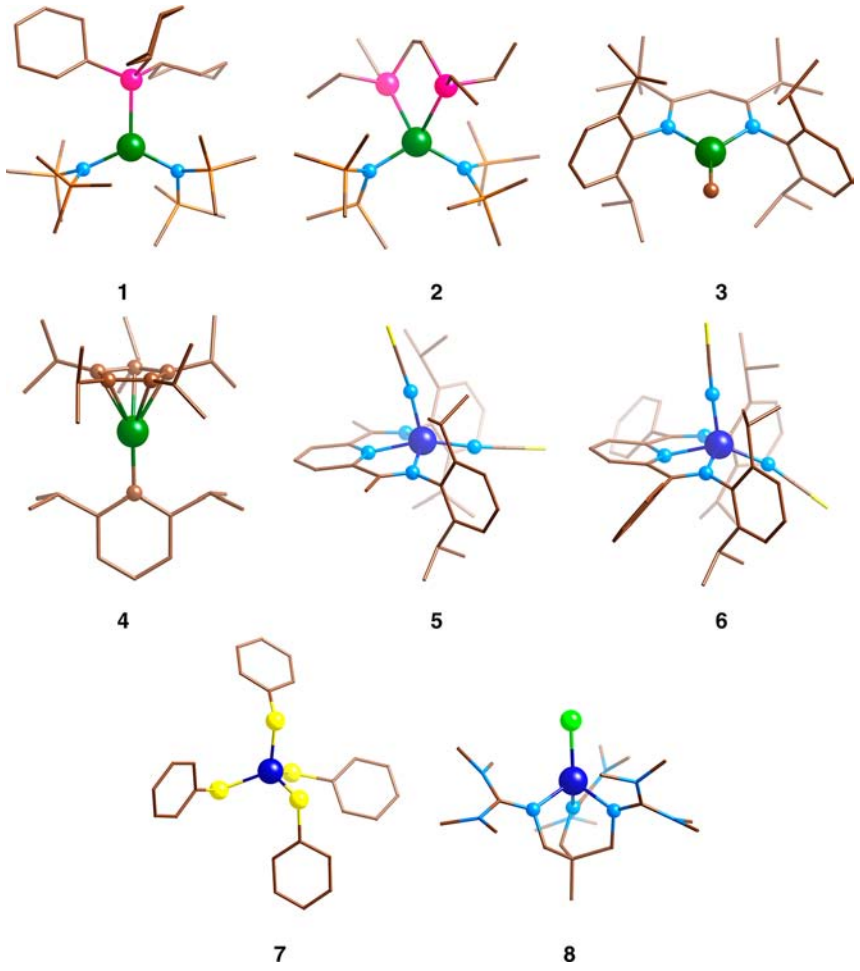


**Figure 1.** Structure determined by single-crystal X-ray diffraction of $[Fe^{II}(N(TMS)_2)_2(PCy_3)]$ (**1**), $[Fe^{II}(N(TMS)_2)_2(depe)]$ (**2**), $[Fe^{II}(Me)L_3]$ ($L_3$: *N*,*N*′-bis(2,6-di-isopropylphenyl)-2,2,6,6-tetramethyl heptane-3,5-di-iminato-*N*,*N*′) (**3**), $[Fe^{II}(iPr_5C_5)(2,6\text{-}iPr_2C_6H_3)]$ (**4**), $[Co^{II}(NCS)_2L_1]$ (**5**), $[Co^{II}(NCS)_2L_2]$ (**6**) ($L_1$ and $L_2$: R = Me or Ph, bis(imino)pyridine, 2,6{ArN═C(R)}$_2$NC$_5$H$_3$), $[Co^{II}(SPh)_4]^{2-}$ (**7**), and $[Co^{II}(Cl)L_4]^+$ (**8**) ($L_4$: 1,1,1-tris-[2*N*-(1,1,3,3-tetramethylguanidino) methyl]ethane). Green, blue, yellow, pink, light-green, orange, light-blue, and brown represent iron, cobalt, sulfur, phosphor, chlorine, silicon, nitrogen, and carbon atoms, respectively. Transition-metal atoms and the ligand atoms linked to the metal are represented with spheres. The other atoms are represented with sticks, while hydrogen atoms are omitted for clarity.

**Table 1. Calculated CASSCF+RASSI Values of *D* and |*E*| (in cm$^{-1}$), ZFS Parameters for Some Fe$^{II}$ and Co$^{II}$ Complexes and First Excitation Energies (in cm$^{-1}$) Calculated at the Spin-Free CASSCF Level**[a]

| complexes | coordination | SMM | $D_{exp}$ ($E_{exp}$) | $D_{calc}$ ($\lvert E_{calc}\rvert$) | $\Delta E_1$ |
|---|---|---|---|---|---|
| **1** $[Fe^{II}(N(TMS)_2)_2(PCy_3)]$ | trigonal planar-3 | yes | -[24] | −54.7 (1.6) | 289 |
| **2** $[Fe^{II}(N(TMS)_2)_2(depe)]$ | tetrahedron-4 | no | -[24] | −9.3 (2.6) | 2805 |
| **3** $[Fe^{II}(Me)L_3]$ | trigonal planar-3 | - | > ± 50[37] | −58.0 (1.0) | 248 |
| **4** $[Fe^{II}(iPr_5C_5)(2,6\text{-}iPr_2C_6H_3)]$ | 6 (5 + 1) | yes | −51.4 (−0.32)[25] | −72.9 (1.1) | 177 |
| **5** $[Co^{II}(NCS)_2L_1]$ | square pyramid-5 | yes | −27.9[30] | −62.1 (10.5) | 923 |
| **6** $[Co^{II}(NCS)_2L_2]$ | square pyramid-5 | yes | −28.0[30] | −121.7 (16.8) | 1197 |
| **7** $[Co^{II}(SPh)_4]^{2-}$ | tetrahedron-4 | yes | −74[29] | −52.2 (0.6) | 389 |
| **8** $[Co^{II}(Cl)L_4]^+$ | tetrahedron-4 | yes | +12.7 (1.2)[31] | +16.9 (1.3) | 2008 |

[a]For each complex we indicate whether mononuclear SMM behavior was detected using ac measurements. TMS = SiMe$_3$; Cy = cyclohexyl; depe = 1,2-bis(diethylphosphino) ethane; $L_1$ and $L_2$: R = Me or Ph, bis(imino)pyridine, 2,6{ArN═C(R)}$_2$NC$_5$H$_3$; $L_3$: *N*,*N*′-bis(2,6-di-isopropylphenyl)-2,2,6,6-tetramethylheptane-3,5-di-iminato-*N*,*N*′; and L4: 1,1,1-tris-[2*N*-(1,1,3,3-tetramethylguanidino)methyl]ethane

relaxation together with huge anisotropic barrier.[10] Since 2008, several mononuclear lanthanide complexes,[11−13] especially those containing Er$^{III}$ and Dy$^{III}$ cations, and some actinide species, with U$^{III}$ and Np$^{III}$ centers,[14−16] have showed similar SMM behavior and have also been called "single-ion magnets", despite that such term was widely employed, we prefer to call them "mononuclear single-molecule magnets". Based on these results it was pointed out that the presence of heavy elements with large spin−orbit made possible the appearance of similar SMM phenomena,[17,18] and their structural and electronic requirements were also analyzed.[19−21] However, in 2010, Long and co-workers synthesized a family of mononuclear tetracoordinate Fe$^{II}$ complexes that show similar magnetic activity by applying a weak static magnetic field reducing this


dx.doi.org/10.1021/ja4015138 | *J. Am. Chem. Soc.* 2013, 135, 7010−7018

way the magnetic tunneling.[22,23] Recently, some mononuclear complexes containing $Fe^{II}$ (and $Fe^{III}$ $S = 3/2$ state) and $Co^{II}$ centers have been reported exhibiting exactly the same behavior.[24−33] The origin of the large anisotropy in first-row mononuclear transition-metal complexes is the presence of low-lying spin−orbit free excited states (CASSCF energies without spin−orbit contributions) with close energies to the ground state; this results in a large contribution to the $D$ value thanks also to their first-order spin−orbit contributions.[34−36]

Following the latest developments, our goals in the present manuscript are to gain understanding of, and thereby rationalize, the origin of magnetic anisotropy in first-row mononuclear transition-metal complexes using theoretical methods and to apply this understanding in the production of new mononuclear SMMs, in a nonserendipitous way, stressing which building blocks will be optimal for achieving very large magnetic anisotropy in polynuclear systems with ferromagnetic or ferrimagnetic spin arrangements.

## RESULTS AND DISCUSSION

The theoretical magnetic anisotropy of a family of tetracoordinate $Fe^{II}$ complexes synthesized by Long and co-workers has previously been analyzed.[35,36] Applying the same method (a CASSCF+RASSI method, see Computational Details section), we analyzed some of the mononuclear $Fe^{II}$ and $Co^{II}$ complexes that have recently been reported to exhibit SMM behavior (Table 1). All the complexes **1**−**7** present negative $D$ values; as opposed to compound **8**, a mononuclear SMM $Co^{II}$ complex, which has a positive $D$ value. It is worth mentioning that systems with positive $D$ values are not generally considered suitable SMM candidates; however, we can now anticipate that systems with half-integer total spin and positive $D$ values may also exhibit such properties (see below).[31,32] From an experimental point of view, the determination of the ZFS parameters using magnetization measurements is not the preferred technique, but large $D$ values prevent the use of the most accurate high-field EPR technique. Taking these drawbacks into account, reasonable agreement between experimental and theoretical results should still be found. In order to facilitate the comparison between theoretical and experimental results, not only through the numerical $D$ and $E$ values of Table 1, we have included as Supporting Information (Figures S1 and S2) the calculated and the experimentally available $\chi T$ and magnetization curves. Regarding this point, the degree of agreement between experimental and theoretical values in Figure S1 ($\chi T$ vs $T$) and S2 ($M$ vs $HT^{-1}$) may be different in some cases because the magnetization figures correspond only to the low-lying states that are populated at low temperature, while the susceptibility curves also include high-temperature contributions. The employed computational approach usually gives better agreement in the magnetization data (see Table S5).

Following the theoretical approach described in the Computational Details section, the calculated results (Table 1) show that SMM behavior should be present in complex **1** ($S = 2$), where the $Fe^{II}$ cations adopt a trigonal planar coordination.[24] It is worth noting that the most studied systems exhibit Jahn−Teller distortions: thus, to describe the coordination mode, for instance in the case of complex **1**, pseudotrigonal planar coordination could be used to indicate the presence of a slightly distorted geometry. The calculated $D$ value for such a system is around $-50$ $cm^{-1}$; similar to the largest value obtained by Long and co-workers for the family of tetracoordinate SMM $Fe^{II}$ complexes that exhibit trigonal pyramid coordination, the $[Fe(tpa^{t\text{-}Bu})]^-$ complex(tpa = tris(pyrrolylmethyl)amine; *t*-Bu = *tert*-butyl).[22,23] For complex **3**, $[Fe^{II}(Me)L_3]$, synthesized by Münck and co-workers,[37] a large $D$ value has been reported, but no AC measurements were carried out. The calculated large negative $D$ value suggests that this complex may also present SMM behavior. In the case of the $[Fe^{II}(N(TMS)_2)_2L]$ family,[24] replacing a monocoordinate phosphine (complex **1** with trigonal planar coordination) by a bidentate one leads to a distorted tetrahedral coordination (complex **2**) which suppresses the SMM behavior, as corroborated by a considerable decrease in the calculated $D$ value. The organometallic complex **4** $[Fe^{II}(iPr_5C_5)(2,6\text{-}iPr_2C_6H_3)]$ with an unusual 6 (5 + 1)[25] coordination, also exhibits SMM behavior in agreement with our calculated large negative $D$ value.

In general, for the $Co^{II}$ complexes, SMM behavior is exhibited in the distorted square pyramid coordination mode[30] (complexes **5** and **6** in Table 1 with calculated large negative $D$ values). Despite the experimental $D$ values for the $[Co^{II}(NCS)_2L]$-type complexes being almost identical, the calculated large $D$ value for complex **5** is consistent with the large experimental relaxation barrier ($U_{eff}$) of 17 $cm^{-1}$, in comparison with complex **6** (11 $cm^{-1}$). The case of the $Co^{II}$ complex **7** is particularly interesting because the complex shows relaxation of the magnetization and a maximum in the $\chi''$ signal without the application of any external dc magnetic field.[29] From a structural point of view, this complex is also remarkable because it shows a distorted tetrahedral structure despite the fact that in theory no Jahn−Teller distortion, neither first nor second order, should be expected for a $d^7$ tetrahedral system. Thus, packing effects or sulfur−sulfur intramolecular interactions may play a significant role in the geometrical distortion. The calculated results (Table 1) also reproduce the large negative value found experimentally. Recently, Plass and co-workers reported two new distorted tetrahedral $Co^{II}$ complexes with negative $D$ values (−35 and −41 $cm^{-1}$) similar to that present in **7** showing slow relaxation with an applied dc field of 400 Oe.[33] Furthermore, the calculated $D$ value properly reproduces the positive $D$ value found for the $Co^{II}$ complex **8** with a distorted tetrahedral coordination which exhibits SMM behavior.[31] It is worth noting that the positive $D$ parameter of such a $Co^{II}$ complex is smaller than the absolute $D$ value of the rest of the mononuclear SMM systems (with negative $D$ parameters). Some attempts to correlate the electronic configuration and the symmetry of a complex with the sign of the magnetic anisotropy were made for $O_h$ and $D_{4h}$ systems by Oshio et al.[38] Recently, McGarvey also analyzed state stability as a function of the geometrical distortion of the coordination sphere for the family of tetracoordinate $Fe^{II}$ complexes synthesized by Long and co-workers, and how the ground state determines the $D$ value.[39] Our goal here is to elucidate the causes of SMM behavior and to elaborate a qualitative approach to predict which ligands, coordination modes, and electronic configurations of the metal center will lead to mononuclear complexes that show this property.

The ZFS parameters ($D$ and $E$) are calculated from the elements of the diagonalized **D** tensor (see eq 2):[8,40,41]

$$D = D_{zz} - (D_{xx} + D_{yy})/2; \quad E = (D_{xx} - D_{yy})/2 \tag{2}$$

The elements of such a tensor can be obtained from


dx.doi.org/10.1021/ja4015138 | J. Am. Chem. Soc. 2013, 135, 7010−7018

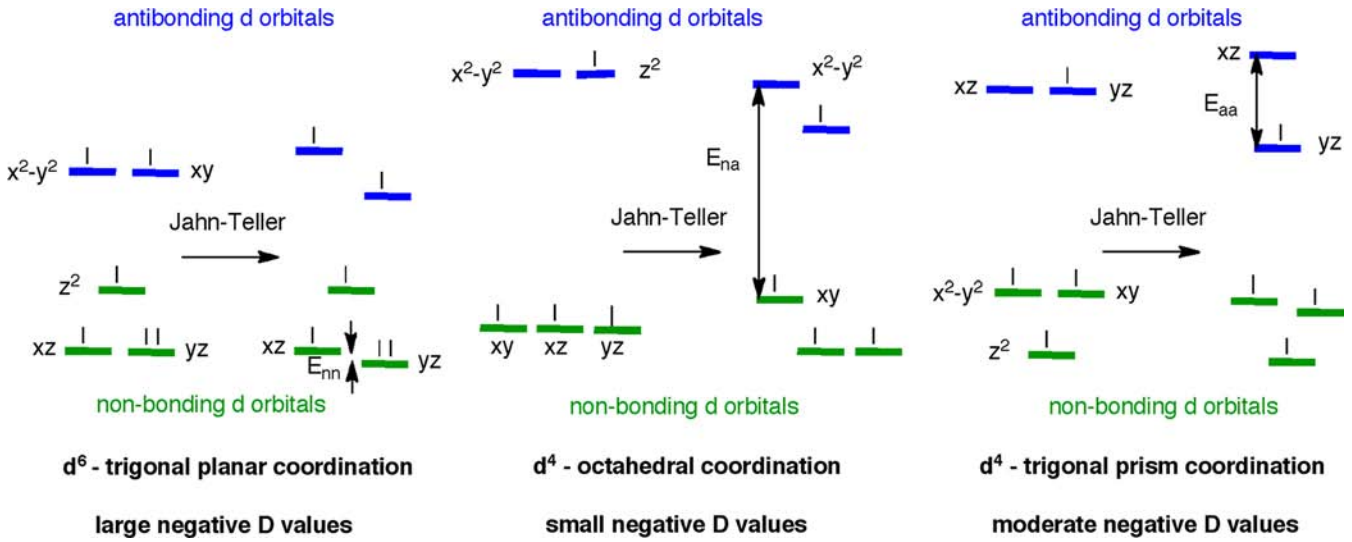


**Figure 2.** Splitting of the d orbitals due to the Jahn–Teller effect for three cases with negative $D$ values: $d^6$-trigonal planar coordination (left), $d^4$-octahedral coordination (middle), and $d^4$-prism trigonal coordination (right). The energy difference indicated by the arrow in each case corresponds to the first excitation that leads to the main contribution to $D_{zz}$ (and $D$, see eqs 1 and 2). The smaller the excitation energy, the larger $|D|$ becomes.

$$D_{kl} = -\frac{\zeta_{\text{eff}}^2}{4S^2}\sum_{i,p}\frac{\langle\varphi_i|l_k|\varphi_p\rangle\langle\varphi_p|l_l|\varphi_i\rangle}{\varepsilon_p - \varepsilon_i} - \frac{\zeta_{\text{eff}}^2}{4S^2}\sum_{p,a}\frac{\langle\varphi_i|l_k|\varphi_a\rangle\langle\varphi_a|l_l|\varphi_i\rangle}{\varepsilon_a - \varepsilon_p} \quad (3)$$

where $\zeta_{\text{eff}}^2$ is the spin–orbital coupling constant, $l_k$ is the $k$-component of the angular momentum operator, and $\varphi$ are the molecular orbitals (with orbital energy $\varepsilon$) with the subindex $i$, $p$, or $a$ to indicate double- and singly-occupied or empty orbitals, respectively. In order to elucidate the origin of the $D$ values, we analyze the different contributions, $D_{ii}$, as a function of the coordination of the metal (splitting of the d orbitals) and the electronic configuration. As was previously observed,[35] for systems **1**–**8** there is also a correlation between the calculated $D$ value and the first excitation energy before applying the spin–orbit corrections (see Table 1). This fact may considerably facilitate the analysis of the results, since we can consider a simple theoretical model in order to estimate the first excitation energies, and such terms will be the most important in determining the $D_{ii}$ components that depend inversely on the energy of the orbitals (or excitation energies). In order to perform the qualitative analysis, we estimated the splitting of the d orbitals using simple extended-Hückel calculations. The splitting of the d orbitals basically depends of the symmetry of the coordination mode, hence, a simple method as extended-Hückel gives a reasonable description of such splitting (see Table S4).

To build the qualitative model, we had to consider the following features: (i) The sign of $D$ will depend on the relative values of the $D_{zz}$ and $(D_{xx} + D_{yy})/2$ terms; thus, if $|D_{zz}|$ is larger than $|(D_{xx} + D_{yy})/2|$, the $D$ value is negative, while the opposite case leads to a positive $D$ value; (ii) the magnitude of the $D_{ii}$ components depends chiefly on two factors: the $m_l$ of the orbitals involved in the integrals with the angular momentum operator (equivalent to the magic pentagon usually employed in EPR to determine the coefficient of the spin–orbit contributions to the anisotropy $g$ components as function of the orbital occupation); and (iii) the difference in energy between such orbitals that can be qualitatively estimated at the extended-Hückel level considering only the excitations with the same multiplicity (see eq 3). Hence, significant contributions to the integrals with the $z$-component of the angular momentum operator, $l_z$, are obtained when the pair of orbitals involved in the first excitations are those with the same $|m_l|$ value, $d_{xy}$ and $d_{x^2-y^2}$ ($m_l = \pm 2$) or $d_{xz}$ with $d_{yz}$ ($m_l = \pm 1$). For the $D_{xx}$ and $D_{yy}$ terms, larger integral values will be related to $m_l$ changes of $\pm 1$ of the orbitals involved.[41]

For instance, an $Fe^{II}$ complex ($d^6$ electronic configuration) displaying trigonal planar coordination (e.g., complexes **1** and **3** in Table 1) presents a Jahn–Teller distortion that breaks the degeneracy of the nonbonding $d_{xz}$ and $d_{yz}$ orbitals (see Figure 2). The first excitation energy will involve these two orbitals which have the same $|m_l|$ value and make a large contribution to the $D_{zz}$ component and, consequently, gives rise to a large negative $D$ value. The nonbonding nature of such orbitals will contribute to high values of $|D|$ because even large geometrical distortions will result in small energy differences between these two d orbitals (eq 3). However, for systems containing a $Mn^{III}$ cation ($d^4$) with elongation of the axial $M–L$ distances which has been widely employed to induce magnetic anisotropy, the $D_{zz}$ contribution will involve large excitation energies from the nonbonding $d_{xy}$ to the antibonding $d_{x^2-y^2}$ orbital (see Figure 2). Such large energy differences in eq 3 will lead to a small negative $D$ value. Thus, we can distinguish three groups of excitation energies as a function of their magnitude: (i) the smallest values are those involving two nonbonding orbitals ($d^6$-trigonal planar coordination, $E_{\text{nn}}$ in Figure 2); (ii) the largest values are those with a nonbonding/antibonding pair of orbitals ($d^4$-octahedral coordination, $E_{\text{na}}$ in Figure 2); and (iii) the pairs of antibonding orbitals that can lead to a moderate splitting of energy ($d^4$-prism trigonal coordination, $E_{\text{aa}}$ in Figure 2) if they are involved in a Jahn–Teller distortion.

Table 2 contains the calculated predictions for high-spin mononuclear complexes with ammonia ligands and employing $Fe^{II}$ cations for the calculations using the extended-Hückel method to estimate the orbital energies (an equivalent table with $\pi$-donor chloride ligands is provided in Table S1). Low-spin cases were not considered because they show only $S = 0$ or 1/2, making the existence of a magnetic anisotropy barrier


dx.doi.org/10.1021/ja4015138 | J. Am. Chem. Soc. 2013, 135, 7010–7018

**Table 2. Estimation of the *D* Values for High-Spin Mononuclear Transition-Metal Complexes with Different Electronic Configurations and Coordination Modes Using Ammonia Ligands (Using the Molecular Orbitals of $Fe^{II}(NH_3)_x$ Models)[a]**


[a]Green and blue squares indicate large and small negative values, in that order, while red and orange represent large and small positive values, respectively. Cases with more than one color indicate that the nondistorted structure has a zero *D* value, and different options are possible depending on the symmetry of the Jahn−Teller distortion.

impossible. Thus, the applicability of such a model is mainly first-row transition-metal complexes, while for the second- and third-rows, only those complexes with low coordination numbers that could reach a high-spin configuration can be considered. For such systems with heavy metals spin values larger than $S = 1$ can be reached with triply degenerated orbitals usually showing high excitations energies but can be compensated by large spin−orbit contributions. For the $d^1$ and $d^9$ electronic configurations, the *D* value is not properly defined, but there is a similar *g* term.[41] As criterion to assign large or small *D* values in Table 2, we have considered that if the energy difference between the two orbitals involved in the eq 3 is larger than 0.03 au the *D* value should be small.

Concerning the information shown in Table 2, there are some examples that can have *D* values of opposite signs depending on the symmetry of the distortion caused by the Jahn−Teller effect; see for instance octahedral $Mn^{III}$ cations, where axial elongation of the ligands leads to small negative *D* values while compression results in positive *D* values (see Table 2). In contrast, there are situations with two possible *D* values of the same sign (e.g., large or small negative values represented by green and blue squares in Table 2, respectively) since the magnitude of *D* will depend on the degree of distortion induced by the Jahn−Teller effect. Hence, if the orbitals involved have a nonbonding character, the excitation energy will be small. However, if two antibonding orbitals ($d^3/d^8$ and $d^4/d^9$ electronic configurations) are involved in the degeneracy, the scale of the distortion may considerably modify the excitation energy and it is difficult to determine whether the value of D will be large or small (see Figure 2). Furthermore, there are


dx.doi.org/10.1021/ja4015138 | J. Am. Chem. Soc. 2013, 135, 7010−7018

some cases with three possible $D$ values due to the presence of triply degenerate orbitals that give different results depending of the relative orbital stabilities caused by the Jahn−Teller distortion.

Our predictions indicate that the $d^6$ electronic configuration with $\sigma$-donor ligands is the most appropriate to lead to SMM with large negative $D$ values. This is consistent with previous explanations where the Jahn−Teller effect involves the two lowest-lying orbitals with nonbonding character. A similar situation was recently reported by Mossin et al.[28] for a trigonal pyramid $Fe^{III}$ complex with spin $S = 3/2$ showing SMM behavior. The $S = 3/2$ value is due to an electronic configuration similar to that of the high-spin $Fe^{II}$ complexes just suppressing the electron in the highest-energy $d_{z^2}$ orbital, while the two lowest-lying orbitals ($d_{xz}$ and $d_{yz}$) bear three electrons, as in high-spin $Fe^{II}$ complexes, resulting in large negative magnetic anisotropy. For $\pi$-donor ligands (see Table S1), if the $d_{xz}$ and $d_{yz}$ (which are often the two lowest-lying degenerate orbitals) are destabilized by the $\pi$-interaction, then in some cases the $d^2/d^7$ electronic configuration becomes the most likely to have large negative anisotropy. The $\pi$-donor ligands induce a reduction of the difference of energy between antibonding d orbitals and the low-energy d orbitals becoming slightly antibonding.

The accuracy of the predictions in Table 2 can be checked by comparison with the previously mentioned mononuclear SMM complexes. Thus, the trigonal planar $Fe^{II}$ complexes (**1** and **3** in Table 1), and the trigonal pyramid $Fe^{II}$ complexes[22,23] correspond to large negative $D$ values in Table 2. Also, the lack of SMM behavior is properly predicted for distorted tetrahedral $Fe^{II}$ complexes (as it happens for **2**). Recently, a new family of linear SMM $Fe^{II}$ complexes with large negative $D$ values has been reported in agreement the predicted behavior in Table 1.[26,27] For high-spin $Co^{II}$ complexes ($d^7$), there are fewer cases with large negative $D$ values (better than the $d^6$ configuration), but with our approach, SMM behavior is also well predicted and comparable to that found in square pyramid $Co^{II}$ complexes (such as **5** and **6**). The occurrence of SMM behavior with large positive $D$ values (less common) requires half-integer S values. However, as we have seen previously, the positive $D$ value for the reported mononuclear $Co^{II}$ SMM complex **8** is smaller than those of negative sign. This may be because the $D_{xx}$ and $D_{yy}$ components are averaged in eq 2. Therefore, high-spin $d^7$ and $d^3$ electronic configurations appear here to be very promising for achieving mononuclear SMM complexes with moderate positive $D$ values. Lately, a distorted octahedral $Co^{II}$ complex with a large positive $D$ value (+98 $cm^{-1}$) showing slow relaxation has been published.[32] Such behavior is in concordance with the predicted value in Table 2 for octahedral $d^7$ $Co^{II}$ cations. Recently, Ruamps et al. reported heptacoordinate $Co^{II}$ complex with a pentagonal bipyramid with a smaller positive D (+31 $cm^{-1}$), but no ac measurements were described to verify the SMM behavior of such system.[42] It is worth noting that for some coordination modes (trigonal planar-3, vacant tetrahedron-3, tetrahedron-4, and those with coordination number 2) the highest energy d orbitals show very weak antibonding behavior. This is the reason why excitation energies from e to $t_2$ orbitals are smaller than expected from the classification proposed in Figure 2. This is crucial for the $Co^{II}$ complex **7** (see Table 1) which adopts a distorted tetrahedral coordination mode, where the highest-energy e orbital ($d_{x^2-y^2}$) is very close to the lowest-energy $t_2$ orbital ($d_{xy}$) thus leading to a large negative $D_{zz}$ (and $D$) term. Finally, the presence of cations with high oxidation states has two opposite contributions: the increase of spin−orbit effects due to the contraction of the atomic core, and also the increase of the energy splittings of the d orbitals (spectrochemical serie of metals) being usually this second factor predominant for high oxidations states. In principle, our qualitative model accurately predicts anisotropy parameters for homoleptic complexes, but due to the similarities between the ligands coordinated to metallic centers, the predictions can be extended to non-homoleptic systems. Thus, from the eight complexes shown in Table 1, only **7** is homoleptic, all of them are correctly predicted in our model in Table 2 (with exception of the **4** complex because its coordination with a ciclopentadiene ligand is not considered there). Nevertheless, it is important to keep in mind that complexes with different ligands which can produce very different energy splitting of the d orbitals will make the application of this straightforward orbital model more difficult. In such cases, individual analysis of the splitting of the d orbitals for each complex will be required.

The final section is devoted to the synthesis and characterization of complexes that, based on our predictive approach, have been proposed as good candidates for SMM behavior. This part of the work was performed with cations that adopt different coordination modes from those of previously reported mononuclear SMMs. Taking into account the nature of the metal, it should be mandatory to have a relatively large total spin ($S$) which therefore involves many states in the magnetic anisotropy barrier. For instance, $d^8$ $Ni^{II}$ complexes with $S = 1$ and only three states are poor candidates for exhibiting SMM properties, despite the fact that for some coordination modes they can present large negative anisotropy (see Table 2). However, the most prolific cation to present SMM behavior in mononuclear systems is $Fe^{II}$, as shown above (Table 1). As candidates we selected the $d^7$ electronic configuration, for instance $Co^{II}$ cations, because SMM behavior could occur either via the trigonal pyramid (large positive $D$ values) or the trigonal prism (large negative $D$ values) coordination modes. In these cases, the coordination is the same as that present in the trigonal pyramid $Fe^{II}$ complexes,[22,23] however the sign will differ in Table 2 predicting large positive $D$ values for $Co^{II}$ complexes, while the equivalent with $Fe^{II}$ shows negative $D$ values. To test this, and after a detailed search in the Cambridge Structural Database,[43] we selected two $Co^{II}$ complexes that had already been reported to adopt the aforementioned coordination spheres, but whose magnetic properties had not previously been measured. In general, the Jahn−Teller effect for these complexes causes distortions that break the orbital degeneracy. The degree of structural distortion is related to the decrease of the $D$ value compared with the maximum value that would correspond to a hypothetically nondistorted structure. Hence, highly symmetric coordination spheres will enhance the SMM behavior. Thus, complexes showing small structural distortions are those expected to present larger $D$ values, and we performed the selection of the complexes with the help of continuous shape measurements.[44,45]

The first system selected was a trigonal pyramid $Co^{II}$ complex previously reported by Borovik and co-workers (**9**, in Figure 3).[46] The synthesis of the complex was repeated (see Supporting Information), and we also performed single crystal X-ray diffraction and magnetic characterization. SQUID studies of complex **9** show no ac magnetic susceptibility signal without an applied external dc field. The ac magnetic susceptibility at 2 K under different external dc fields was investigated, and as


dx.doi.org/10.1021/ja4015138 | J. Am. Chem. Soc. 2013, 135, 7010−7018

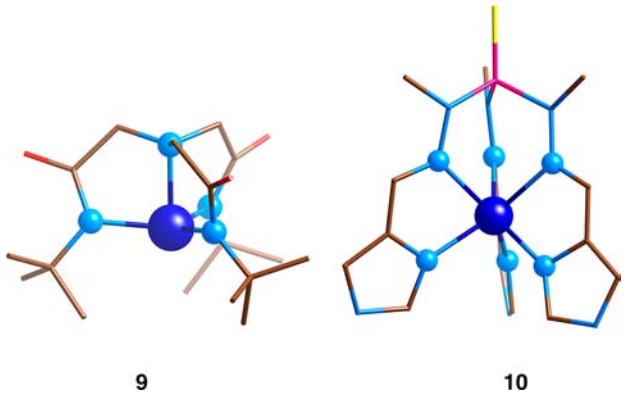


**Figure 3.** Structure determined by single-crystal X-ray diffraction of $K\{Co(N[CH_2C(O)NC(CH_3)_3]_3)\}$ (**9**) and $[Co(P(S)\{[N(CH_3)N{=}CHC_3N_2H_3]_3)\}][(NO_3)_2]$ (**10**). Blue, yellow, light-pink, red, light-blue, and brown represent cobalt, sulfur, phosphor, oxygen, nitrogen, carbon, and hydrogen atoms, respectively. Transition-metal and ligand atoms linked to the metal are represented with spheres. The other atoms are represented with sticks, while hydrogen atoms are omitted for clarity.

shown in Figure S4, a peak appeared at 190 Hz under a field of 250 Oe. This peak slightly shifts to lower frequencies and intensifies with an increase in the applied dc field to 1500 Oe. At this applied dc field the dependence with the temperature was investigated, and the ac magnetic susceptibility showed the characteristic dependence on the out-of-phase ($\chi''$) and in-phase ($\chi'$) susceptibilities with the frequency (Figures 4 and S5) due to the slow relaxation of the magnetization and SMM behavior.

In order to check whether the relaxation processes were thermally activated, Cole−Cole plots were fitted using the generalized Debye model[47] (Figure S6), and the relaxation times ($\tau$) together with the $\alpha$ parameter values were obtained. The logarithmic relaxation time versus $1/T$ was represented (Figure S7), and the curve presents a complex dependence probably due to the concurrence of different mechanisms (quantum tunneling, direct, Raman, Orbach).[26,27] Despite such dependence a characteristic Arrhenius linearity was assumed between 2.75 and 5 K. The application of the Arrhenius law gives an effective barrier ($U_{eff}$) of 8.7 $cm^{-1}$ and a $\tau_o$ of $8 \times 10^{-6}$ s (with $\alpha$ values between 0.09 and 0.02). From the dependence of the magnetization on the temperature and magnetic field, the $D(|E|)$ value of +16(0.0) $cm^{-1}$ was extracted[45] (Figure S8) in agreement with the CASSCF-RASSI results $D(|E|)$ = +36.9(0.5) $cm^{-1}$ and the predicted value in Table 2. It is important to keep in mind the uncertainties in the determination of the $D$ values for this kind of system, as mentioned above, due to the limitations of the Hamiltonian employed.[34]

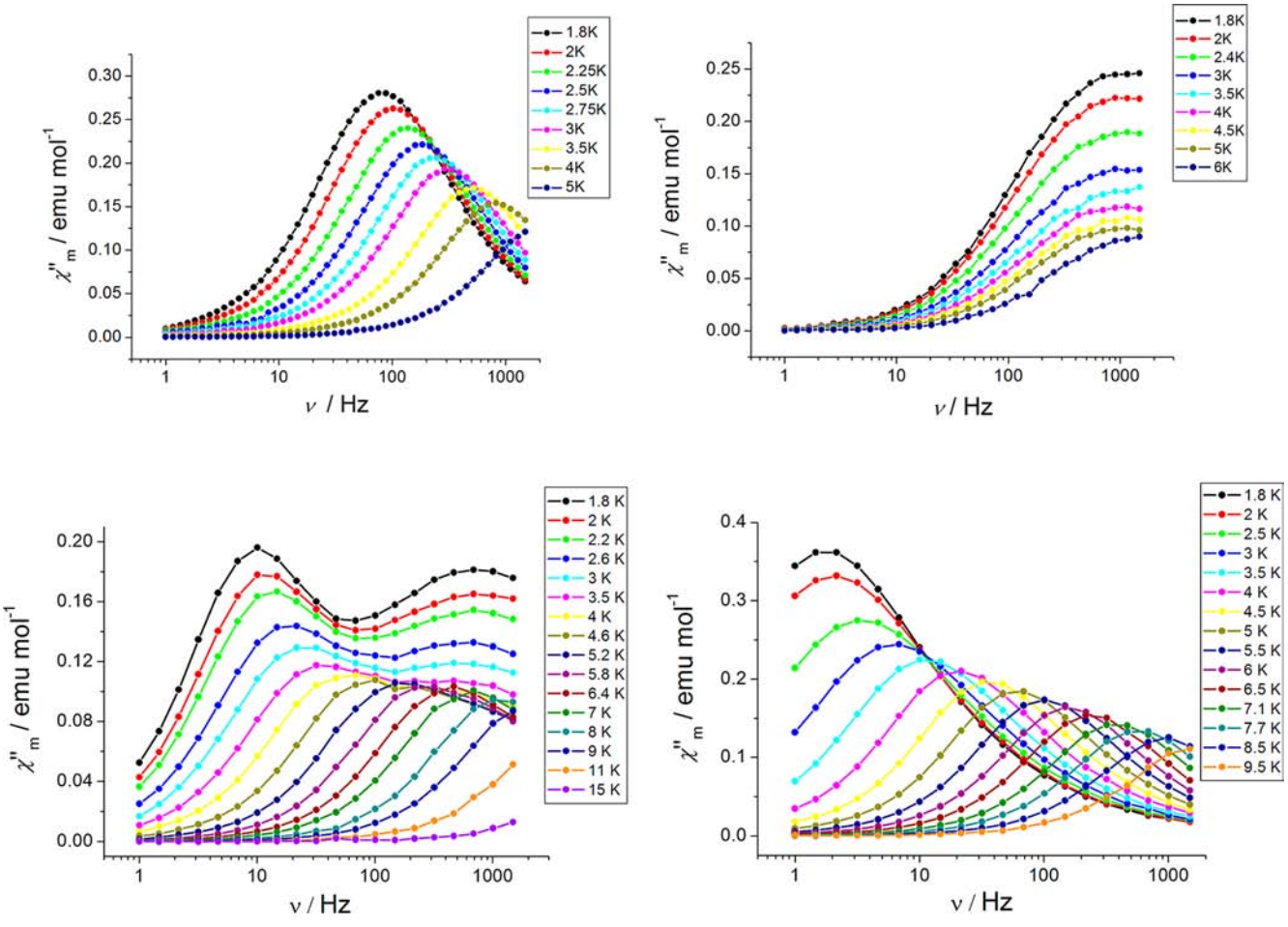


**Figure 4.** Variable-frequency out of phase ac susceptibility data of complex **9** at 1500 Oe applied dc field (top left) and of the complex **10** without an applied dc field (top right), for the same complex **10** with 375 Oe applied dc field (down left) and with 2000 Oe applied dc field (down right).


dx.doi.org/10.1021/ja4015138 | J. Am. Chem. Soc. 2013, 135, 7010−7018

The following system chosen for such studies was a trigonal prism $Co^{II}$ complex[49] (**10** in Figure 3), which according to the predictions in Table 2 should present a large negative $D$ value, in contrast with octahedral $Co^{II}$ complexes that exhibit a large positive $D$ value. The complex was synthesized following a procedure similar to that previously reported (see Supporting Information). The magnetic studies of complex **10** showed an ac magnetic susceptibility signal without an external applied static dc field, but no maximum in the $\chi''$ signal was found (Figure 4). However, when different small dc fields are applied, the $\chi''$ versus frequency signal at 2 K dramatically changes with the magnitude of the applied dc field (Figure S11). The signal observed without dc field shows a maximum and diminished when the dc field was increases; from 2000 Oe the signal disappears. On the other hand, another peak at 10 Hz appeared with the application of the dc field, the increase of the dc field shift the peak to lower frequencies enhancing in magnitude. Due to this behavior, the variations of the $\chi''$ versus frequency signal with the temperature at two different dc applied fields were studied. At 375 Oe, $\chi''$ showed the existence of two peaks and at 2000 Oe, where $\chi''$ only presented the lower frequency peak. When a dc field of 375 Oe was applied, the $\chi''$ versus frequency signal at 1.8 K showed two peaks at 700 and 10 Hz (Figure 4). When the temperature was increased to 3 K, the higher-frequency peak does not shown dependence with the temperature, indicating a quantum regime, while the lower-frequency peak showed a shift in the maxima to higher frequencies, which indicates a thermal activated regime. At higher temperatures, the two peaks are indistinguishable. At 2000 Oe, the $\chi''$ versus frequency signal for complex **10** only showed one peak (Figure 4), and when the temperature was increased, the peak shifted to higher frequencies, which again indicates a thermal activated regime and confirms the predicted SMM behavior and should be the first example of trigonal prism mononuclear SMM. As before, the Cole−Cole plots were fitted[47] (Figure S14), and the relaxation times and $\alpha$ parameters calculated. The logarithmic relaxation time versus $1/T$ was represented (Figure S15). Characteristic Arrhenius linearity was observed between 5 and 9.5 K giving a $U_{eff}$ of 23 $cm^{-1}$ and a $\tau_o$ of $4 \times 10^{-6}$ s (with $\alpha$ values between 0.14 and 0.02). From the dependence of the magnetization on temperature and the magnetic field, the $D(|E|)$ value of $-72(7)$ $cm^{-1}$ was arrived at[45] (Figure S16) in agreement with the prediction in Table 2 and slightly slower than the CASSCF-RASSI results: $D(|E|) = -141(2.2)$ $cm^{-1}$.

## CONCLUSIONS

In this work, we show that CASSCF methods can provide a semiquantitative estimation of the ZFS parameters ($D$ and $E$) for mononuclear first-row transition-metal complexes. We also corroborate the existence of a correlation between the magnetic anisotropy, quantified by means of the $D$ parameters, and the first excitation energy. In order to predict the magnetic anisotropy for any mononuclear complex, we employed such a correlation using the extended-Hückel approach to determine the energy splitting of the d orbitals qualitatively. The combination of the results with the analysis of the values of the angular momentum integrals allowed us to predict the magnetic anisotropy for mononuclear complexes, by taking into account their coordination mode and the electronic configuration of the metal, showing that mononuclear complexes with high coordination numbers can also present SMM behavior. Finally, we validated such predictions with the mononuclear SMMs described in the literature and two previously reported $Co^{II}$ complexes, whose magnetic properties we characterized to confirm the predicted SMM behavior. Thus, the use of such information and the proposed procedure may forward the rational design either of new mononuclear SMMs or of polynuclear complexes using the appropriate mononuclear building blocks.

## COMPUTATIONAL DETAILS

The ZFS parameters were obtained using the procedure described by Maurice et al.,[50,51] first performing a CASSCF calculation, and second the energy of these CASSCF states was mixed within the SO-RASSI approach (MOLCAS code).[52] We used an all electron ANO-RCC basis set: Fe and Co atoms (6s5p4d2f), N and O (4s3p1d), C (3s2p), and H (2s) with an active space considering the six d (or seven) electrons of the $Fe^{II}$ (or $Co^{II}$) centers and the five d orbitals. Extended-Hückel calculations for the model structures were performed using Gaussian09 code.[53]

## EXPERIMENTAL SECTION

Characterization. Magnetic measurements were carried out using a Quantum Design MPMS SQUID magnetometer. Analysis was performed on crushed polycrystalline samples of 23 mg for **9** and 34 mg for **10**, respectively. The ac magnetic susceptibility measurements were carried out by applying an ac field of 4 Oe, with ac frequencies from 1 to 1500 Hz and the external dc field indicated in the text. The reduced magnetization $M/N\mu_B$ vs $H/T$ plots were made at applied fields of 0.5, 1, 2, 3, 4, and 5 T, respectively, in the 1.8−6.8 K range for complexes **9** and **10**. The fitting of the data was performed with a full matrix diagonalization approach.[45] X-ray diffraction details are included ion the Supporting Information. CCDC-894342 and CCDC-894343 contain the supplementary crystallographic data for **9** and **10**. These data can be obtained free of charge via http://www.ccdc.cam.ac.uk/conts/retrieving.html or from the Cambridge Crystallographic Data Centre, 12 Union Road, Cambridge CB2 1EZ, UK; fax: +44 (0) 1223−336−033; or e-mail: deposit@ccdc.cam.ac.uk.

## ASSOCIATED CONTENT

### Supporting Information

Predicted $D$ values for high-spin mononuclear transition-metal complexes with $\pi$-donor chloride ligands (Table S1). Details of the synthesis and characterization of complexes **9** and **10**. X-ray data of complexes **9** and **10** (Tables S2 and S3). Comparison of energies of EH molecular orbitals and CASSCF energies (Table S4). Comparison of calculated and experimental magnetic properties of complexes **1**−**10** (Figures S1, S2 and Table S5). Magnetic characterization of complexes **9** and **10** (Figures S3−S16). This information is available free of charge via the Internet at http://pubs.acs.org.

## AUTHOR INFORMATION

### Corresponding Author

eliseo.ruiz@qi.ub.es

### Notes

The authors declare no competing financial interest.

## ACKNOWLEDGMENTS

The research reported here was supported by the Spanish Ministerio de Economía y Competitividad (grants CTQ2011-23862-C02-01 and CTQ2009-06959/BQU) and the regional Generalitat de Catalunya authority (2009SGR-1459). S.G.C. thanks the Spanish Ministerio de Educación, Cultura y Deporte for a predoctoral fellowship. The authors thankfully acknowledge the computer resources, technical expertise, and assistance provided by the CESCA. Structural and magnetic character-

ization of the samples were carried out in the CCiT (Centres Científics i Tecnològics) of the Universitat de Barcelona.

## REFERENCES


(1) Gatteschi, D.; Sessoli, R. *Angew. Chem., Int. Ed.* **2003**, *42*, 268.
(2) Gatteschi, D.; Sessoli, R.; Villain, J. *Molecular Nanomagnets*; Oxford University Press: Oxford, U.K., 2006.
(3) Boca, R. *Coord. Chem. Rev.* **2004**, *248*, 757.
(4) Sessoli, R.; Gatteschi, D.; Caneschi, A.; Novak, M. A. *Nature* **1993**, *365*, 141.
(5) Aromi, G.; Brechin, E. K. *In Single-Molecule Magnets and Related Phenomena*; Winpenny, R., Ed.; Springer-Verlag: Berlin, Germany, **2006**; Vol. *122*, p 1.
(6) Milios, C. J.; Inglis, R.; Vinslava, A.; Bagai, R.; Wernsdorfer, W.; Parsons, S.; Perlepes, S. P.; Christou, G.; Brechin, E. K. *J. Am. Chem. Soc.* **2007**, *129*, 12505.
(7) Milios, C. J.; Vinslava, A.; Wernsdorfer, W.; Moggach, S.; Parsons, S.; Perlepes, S. P.; Christou, G.; Brechin, E. K. *J. Am. Chem. Soc.* **2007**, *129*, 2754.
(8) Cirera, J.; Ruiz, E.; Alvarez, S.; Neese, F.; Kortus, J. *Chem.—Eur. J.* **2009**, *15*, 4078.
(9) Ishikawa, N.; Sugita, M.; Ishikawa, T.; Koshihara, S.; Kaizu, Y. *J. Am. Chem. Soc.* **2003**, *125*, 8694.
(10) Branzoli, F.; Carretta, P.; Filibian, M.; Zoppellaro, G.; Graf, M. J.; Galan-Mascaros, J. R.; Fuhr, O.; Brink, S.; Ruben, M. *J. Am. Chem. Soc.* **2009**, *131*, 4387.
(11) AlDamen, M. A.; Clemente-Juan, J. M.; Coronado, E.; Marti-Gastaldo, C.; Gaita-Arino, A. *J. Am. Chem. Soc.* **2008**, *130*, 8874.
(12) Jiang, S.-D.; Wang, B.-W.; Su, G.; Wang, Z.-M.; Gao, S. *Angew. Chem., Int. Ed.* **2010**, *49*, 7448.
(13) Jiang, S.-D.; Wang, B.-W.; Sun, H.-L.; Wang, Z.-M.; Gao, S. *J. Am. Chem. Soc.* **2011**, *133*, 4730.
(14) Rinehart, J. D.; Long, J. R. *J. Am. Chem. Soc.* **2009**, *131*, 12558.
(15) Antunes, M. A.; Pereira, L. C. J.; Santos, I. C.; Mazzanti, M.; Marcalo, J.; Almeida, M. *Inorg. Chem.* **2011**, *50*, 9915.
(16) Magnani, N.; Apostolidis, C.; Morgenstern, A.; Colineau, E.; Griveau, J. C.; Bolvin, H.; Walter, O.; Caciuffo, R. *Angew. Chem., Int. Ed.* **2011**, *50*, 1696.
(17) Rinehart, J. D.; Long, J. R. *Chem. Sci.* **2011**, *2*, 2078.
(18) Palii, A.; Tsukerblat, B.; Klokishner, S.; Dunbar, K. R.; Clemente-Juan, J. M.; Coronado, E. *Chem. Soc. Rev.* **2011**, *40*, 3130.
(19) Baldovi, J. J.; Borras-Almenar, J. J.; Clemente-Juan, J. M.; Coronado, E.; Gaita-Arino, A. *Dalton Trans.* **2012**, *41*, 13705.
(20) Baldovi, J. J.; Cardona-Serra, S.; Clemente-Juan, J. M.; Coronado, E.; Gaita-Arino, A. *Chem. Sci.* **2013**, *4*, 938.
(21) Baldovi, J. J.; Cardona-Serra, S.; Clemente-Juan, J. M.; Coronado, E.; Gaita-Arino, A.; Palii, A. *Inorg. Chem.* **2012**, *51*, 12565.
(22) Freedman, D. E.; Harman, W. H.; Harris, T. D.; Long, G. J.; Chang, C. J.; Long, J. R. *J. Am. Chem. Soc.* **2010**, *132*, 1224.
(23) Harman, W. H.; Harris, T. D.; Freedman, D. E.; Fong, H.; Chang, A.; Rinehart, J. D.; Ozarowski, A.; Sougrati, M. T.; Grandjean, F.; Long, G. J.; Long, J. R.; Chang, C. J. *J. Am. Chem. Soc.* **2010**, *132*, 18115.
(24) Lin, P.-H.; Smythe, N. C.; Gorelsky, S. I.; Maguire, S.; Henson, N. J.; Korobkov, I.; Scott, B. L.; Gordon, J. C.; Baker, R. T.; Murugesu, M. *J. Am. Chem. Soc.* **2011**, *133*, 15806.
(25) Weismann, D.; Sun, Y.; Lan, Y.; Wolmershaeuser, G.; Powell, A. K.; Sitzmann, H. *Chem.—Eur. J.* **2011**, *17*, 4700.
(26) Atanasov, M.; Zadrozny, J. M.; Long, J. R.; Neese, F. *Chem. Sci.* **2013**, *4*, 139.
(27) Zadrozny, J. M.; Atanasov, M.; Bryan, A. M.; Lin, C. Y.; Rekken, B. D.; Power, P. P.; Neese, F.; Long, J. R. *Chem. Sci.* **2013**, *4*, 125.
(28) Mossin, S.; Tran, B. L.; Adhikari, D.; Pink, M.; Heinemann, F. W.; Sutter, J.; Szilagyi, R. K.; Meyer, K.; Mindiola, D. J. *J. Am. Chem. Soc.* **2012**, *134*, 13651.
(29) Zadrozny, J. M.; Long, J. R. *J. Am. Chem. Soc.* **2011**, *133*, 20732.
(30) Jurca, T.; Farghal, A.; Lin, P.-H.; Korobkov, I.; Murugesu, M.; Richeson, D. S. *J. Am. Chem. Soc.* **2011**, *133*, 15814.
(31) Zadrozny, J. M.; Liu, J.; Piro, N. A.; Chang, C. J.; Hill, S.; Long, J. R. *Chem. Commun.* **2012**, *48*, 3927.
(32) Vallejo, J.; Castro, I.; Ruiz-Garcia, R.; Cano, J.; Julve, M.; Lloret, F.; De Munno, G.; Wernsdorfer, W.; Pardo, E. *J. Am. Chem. Soc.* **2012**, *134*, 15704.
(33) Buchholz, A.; Eseola, A. O.; Plass, W. *C. R. Chim.* **2012**, *15*, 929.
(34) Palii, A. V.; Clemente-Juan, J. M.; Coronado, E.; Klokishner, S. I.; Ostrovsky, S. M.; Reu, O. S. *Inorg. Chem.* **2010**, *49*, 8073.
(35) Cremades, E.; Ruiz, E. *Inorg. Chem.* **2011**, *50*, 4016.
(36) Atanasov, M.; Ganyushin, D.; Pantazis, D. A.; Sivalingam, K.; Neese, F. *Inorg. Chem.* **2011**, *50*, 7460.
(37) Andres, H.; Bominaar, E. L.; Smith, J. M.; Eckert, N. A.; Holland, P. L.; Munck, E. *J. Am. Chem. Soc.* **2002**, *124*, 3012.
(38) Oshio, H.; Nakano, M. *Chem.—Eur. J.* **2005**, *11*, 5178.
(39) McGarvey, B. R.; Telser, J. *Inorg. Chem.* **2012**, *51*, 6000.
(40) Neese, F. *J. Chem. Phys.* **2007**, *127*, 164112.
(41) Neese, F.; Solomon, E. I. *In Magnetism: Molecules to Materials*; Miller, J. S., Drillon, M., Eds.; Wiley-VCH: Weinheim, Germany, 2003; Vol. *4*, p 345.
(42) Ruamps, R.; Batchelor, L. J.; Maurice, R.; Gogoi, N.; Jimenez-Lozano, P.; Guihery, N.; de Graaf, C.; Barra, A. L.; Sutter, J. P.; Mallah, T. *Chem.—Eur. J.* **2013**, *19*, 950.
(43) Allen, F. H. *Acta Cryst. B* **2002**, *58*, 380.
(44) Alvarez, S.; Alemany, P.; Casanova, D.; Cirera, J.; Llunell, M.; Avnir, D. *Coord. Chem. Rev.* **2005**, *249*, 1693.
(45) Llunell, M.; Casanova, D.; Cirera, J.; Alemany, P.; Alvarez, S. *Shape program*, version 2; Universitat de Barcelona: Barcelona, Spain, 2010.
(46) Ray, M.; Hammes, B. S.; Yap, G. P. A.; Rheingold, A. L.; Borovik, A. S. *Inorg. Chem.* **1998**, *37*, 1527.
(47) Aubin, S. M. J.; Sun, Z.; Pardi, L.; Krzystek, J.; Folting, K.; Brunel, L.-C.; Rheingold, A. L.; Christou, G.; Hendrickson, D. N. *Inorg. Chem.* **1999**, *38*, 5329.
(48) Rivière, E. *Software to extract D and E values*; Université Paris Sud: Orsay, France.
(49) Chandrasekhar, V.; Azhakar, R.; Pandian, B. M.; Boomishankar, R.; Steiner, A. *Dalton Trans.* **2008**, 5962.
(50) Maurice, R.; Bastardis, R.; Ade Graaf, C.; Suaud, N.; Mallah, T.; Guihery, N. J. *Chem. Theory Comput.* **2009**, *5*, 2977.
(51) Maurice, R.; Guihery, N.; Bastardis, R.; de Graaf, C. J. *Chem. Theory Comput.* **2010**, *6*, 55.
(52) Aquilante, F.; De Vico, L.; Ferre, N.; Ghigo, G.; Malmqvist, P. A.; Neogrady, P.; Pedersen, T. B.; Pitonak, M.; Reiher, M.; Roos, B. O.; Serrano-Andres, L.; Urban, M.; Veryazov, V.; Lindh, R. *J. Comput. Chem.* **2010**, *31*, 224.
(53) Frisch, M. J.; Trucks, G. W.; Schlegel, H. B.; Scuseria, G. E.; Robb, M. A.; Cheeseman, J. R.; Scalmani, G.; Barone, V.; Mennucci, B.; Petersson, G. A.; Nakatsuji, H.; Caricato, M.; Li, X.; Hratchian, H. P.; Izmaylov, A. F.; Bloino, J.; Zheng, G.; Sonnenberg, J. L.; Hada, M.; Ehara, M.; Toyota, K.; Fukuda, R.; Hasegawa, J.; Ishida, M.; Nakajima, T.; Honda, Y.; Kitao, O.; Nakai, H.; Vreven, T.; Montgomery, J. A., Jr.; Peralta, J. E.; Ogliaro, F.; Bearpark, M.; Heyd, J. J.; Brothers, E.; Kudin, K. N.; Staroverov, V. N.; Kobayashi, R.; Normand, J.; Raghavachari, K.; Rendell, A.; Burant, J. C.; Iyengar, S. S.; Tomasi, J.; Cossi, M.; Rega, N.; Millam, N. J.; Klene, M.; Knox, J. E.; Cross, J. B.; Bakken, V.; Adamo, C.; Jaramillo, J.; Gomperts, R.; Stratmann, R. E.; Yazyev, O.; Austin, A. J.; Cammi, R.; Pomelli, C.; Ochterski, J. W.; Martin, R. L.; Morokuma, K.; Zakrzewski, V. G.; Voth, G. A.; Salvador, P.; Dannenberg, J. J.; Dapprich, S.; Daniels, A. D.; Farkas, Ö.; Foresman, J. B.; Ortiz, J. V.; Cioslowski, J.; Fox, D. J. *Gaussian 09*, revision A.01; Gaussian Inc.: Wallingford, CT, 2010.